Metabolic and Population Profiles of Active Subseafloor Autotrophs in Young Oceanic Crust at Deep-Sea Hydrothermal Vents

Sabrina M. Elkassas,[a,b,#] Caroline S. Fortunato,[c,d] Sharon L. Grim,[a] David A. Butterfield,[e] James F. Holden,[f] Joseph J. Vallino,[c] Christopher K. Algar,[g] Lisa Zeigler Allen,[h,i] Benjamin T. Larson,[e] Giora Proskurowski,[e,j] Emily Reddington,[c,k] Lucy C. Stewart,[f,l] Begum Topçuoğlu,[f,m] and Julie A. Huber[a,#]

[a]Department of Marine Chemistry and Geochemistry, Woods Hole Oceanographic Institution, Woods Hole, MA, USA

[b]Department of Earth, Atmospheric, and Planetary Sciences, Massachusetts Institute of Technology, Cambridge, MA, USA

[c]Ecosystems Center, Marine Biological Laboratory, Woods Hole, MA, USA

[d]Present address: Department of Biology, Widener University, Chester, PA, USA

[e]Cooperative Institute for Climate, Ocean & Ecosystem Studies, University of Washington, Seattle, WA, USA

[f]Department of Microbiology, University of Massachusetts Amherst, Amherst, MA, USA

[g]Department of Oceanography, Dalhousie University, Halifax, Nova Scotia, Canada

[h]Scripps Institution of Oceanography, University of California, San Diego, La Jolla, CA, USA

[i]Department of Microbial and Environmental Genomics, J. Craig Venter Institute, La Jolla, CA, USA.

[j]Present address: MarqMetrix, ThermoFisher Scientific, Seattle, WA

[k]Present address: Great Pond Foundation, Edgartown, MA, USA

[l]Present address: New Zealand Association of Scientists, Wellington, NZ

[m]Present address: Bristol Myers Squibb, Summit, NJ, USA

Running Head: RNA-SIP of microbial autotrophs at hydrothermal vents

[#]Address correspondence to Sabrina Elkassas, elks@mit.edu and Julie Huber, jhuber@whoi.edu

Sabrina Elkassas and Caroline Fortunato contributed equally to this work. Julie Huber, the final author listed, is the Principal Investigator on this project.

ABSTRACT

At deep-sea hydrothermal vents, magmatically driven rock-water reactions in the crust generate gases and other reduced compounds that subseafloor microorganisms use for chemolithoautotrophy. In this study, microbial autotrophs from three diffuse flow hydrothermal vents at Axial Seamount in 2013 and 2014 were isotopically labeled using RNA Stable Isotope Probing (RNA-SIP), targeting subseafloor autotrophic mesophiles (30°C), thermophiles (55°C), and hyperthermophiles (80°C). We constructed taxonomic and functional profiles of active chemolithoautotrophs, examined population distributions across sites, and linked primary producers to their specific metabolic strategies within the subseafloor community. Dominant autotrophs exhibited hydrogen-dependent dissimilatory metabolisms such as sulfur and nitrate reduction and methanogenesis, as well as microaerophilic sulfide oxidation even at 80°C, consistent with fluid chemistries at each site. While hydrogenotrophic methanogenic archaea such as *Methanothermococcus* were restricted in their distribution and activity, hydrogenotrophic sulfur and nitrate reducers from the Aquificota (*Thermovibrio*), Campylobacterota (Nautiliaceae, *Hydrogenimonas*, and Desulfurobacteriaceae) were consistently active and present at all sites and years at both the population and community levels. Hydrogenase transcripts were significantly differentially expressed, and diverse hydrogenases were found in metagenome-assembled genomes of Aquificota members, highlighting the importance and versatility of their hydrogen utilization strategies which likely contribute to their cosmopolitan distribution across

geochemically disparate subseafloor sites. Together, this study provides new insights into the functional dynamics and distribution of key subseafloor autotrophic microbial communities in young oceanic crust at deep-sea hydrothermal vents.

Keywords: deep-sea hydrothermal vents, RNA-SIP, chemolithoautotrophy, diffuse flow

IMPORTANCE

Deep-sea hydrothermal vents are hotspots for life in the dark ocean, where rich animal ecosystems are supported by microbial primary producers utilizing the abundant chemical energy supplied by high-temperature water-rock reactions. Despite increasing knowledge about the geochemistry and microbiology of deep-sea hydrothermal vents, there is still a gap in our understanding of the key microbial players who fix much of the carbon at these sites, especially in the productive subseafloor. In this study, stable isotope probing was used to label active microbial autotrophs in diffuse flow venting fluids from three sites over two years and was combined with metatranscriptomic sequencing to identify their specific metabolic strategies. This research highlights the microbial community composition, function, gene regulation, and population dynamics that enable hydrothermal ecosystems to persist.

INTRODUCTION

Deep-sea hydrothermal systems span large temperature and geochemical gradients, from cold, oxidized seawater to hot, highly reduced hydrothermal fluid produced by rock-water reactions. These systems host a wide diversity of microbial niches, many of which are powered by chemolithoautotrophy, including chimneys, animals, venting fluids, hydrothermal plumes, mats, and the subseafloor (1). Mixing zones at and below the seafloor can be sampled through diffuse

70 flow vents (~5-120°C), providing a glimpse into the subseafloor habitat within oceanic crust, one
71 of the most productive microbial niches in the vent environment (2-11).

72 Phylogenetic, metagenomic, and metatranscriptomic studies of diffuse flow microbes have
73 expanded our knowledge on the composition and variability of these communities over time and
74 space, spanning a variety of tectonic settings, host rock types, and geochemical regimes (e.g. 1, 7-
75 10, 12-22). The diffuse flow microbial communities identified in these studies include a mix of
76 seawater, seafloor, and subseafloor populations that inhabit a wide range of temperatures along
77 diverse geochemical gradients, making it difficult to identify active subseafloor residents and the
78 factors controlling their distribution and metabolisms. However, the recent application of stable
79 isotope probing, including RNA Stable Isotope Probing (RNA-SIP), is providing new insights into
80 microbial activity in the dynamic and hard-to-access subseafloor environment (8, 11, 23-24).

81 RNA-SIP is an experimental technique by which isotopically labeled substrate is added to
82 environmental samples at near-natural conditions, incubated, and the label incorporation is probed
83 at the genetic level through sequencing of transcripts (8, 25-26). Resulting isotope-enriched RNA-
84 SIP metatranscriptomes reveal the identity and functional attributes of the microbes that
85 incorporate the labeled substrates in each community under defined experimental conditions (8,
86 25-26). The first deep-sea application of this method was at Axial Seamount (Juan de Fuca Ridge
87 NE Pacific Ocean), a site with a long record of integrated studies of diffuse vent fluid that
88 document microbial communities composed of Campylobacterota, Aquificota, and methanogenic
89 archaea, carrying out sulfide and hydrogen oxidation, sulfur and nitrate reduction, and
90 methanogenesis (6, 8, 10, 12, 15, 17, 18, 22). In this initial RNA-SIP study, diffuse fluid from one
91 site in one year was incubated with labeled bicarbonate to target autotrophs at mesophilic,
92 thermophilic, and hyperthermophilic growth regimes in the subseafloor (8). Results revealed the

power of RNA-SIP in this environment by reducing the complexity of the mixed diffuse fluids, pinpointing the distinct genera and metabolisms that comprised the subseafloor autotrophic community under each growth regime at this site. At 30°C and 55°C, Campylobacterota were dominant, oxidizing hydrogen and primarily reducing nitrate, while methanogenic archaea were the only autotrophs present at 80°C. The method was later used at multiple hydrothermal vent sites along the Mariana back-arc, where RNA-SIP incubations at 55°C and 80°C indicated that autotrophic Campylobacterota were active and present at all but one sampled vent, which instead had a high abundance and activity of autotrophic Aquificota. These differences were attributed to variation in hydrothermal activity due to underlying tectonic setting (23).

Given the ability of RNA-SIP to link specific microbial activities to their metabolisms, genes, and populations across different incubation conditions, we applied this methodology to address hypotheses about the distribution and activity of subseafloor autotrophs in three diffuse flow vents at Axial Seamount: Marker 113, Anemone, and Marker 33. These vents were chosen because they are situated among different vent fields within the Axial caldera, and they are geochemically and microbiologically distinct (10, 27-28). While all of Axial is hosted in basalt, Marker 33 and Marker 113 vent directly from the seafloor lava flows, while Anemone vents through a sulfide mound atop lava flows (10, 27). Fortunato *et al*. (2018) (10) used metagenomics and metatranscriptomics coupled to geochemistry to study the unmanipulated venting fluids from the three sites in three consecutive years. The study found that each site maintained their specific microbial communities and populations over time, but with spatially distinct taxonomy, metabolic potential, and gene transcription profiles. Some organisms and metabolisms were restricted in distribution, such as hydrogenotrophic methanogens, which was linked to host vent chemistry and venting style (10, 28).

116 Building on this legacy of diffuse fluid research at Axial Seamount, we present two years
117 of RNA-SIP data from these same three diffuse flow vent sites at three temperatures to examine
118 how the active microbial subseafloor autotrophs at Axial Seamount vary with temperature, fluid
119 chemistry, geology of the vent (sulfide vs. basalt), space, and time. We hypothesized that the
120 subseafloor autotrophic microbial population structure at each vent and temperature would be
121 distinct, with transcriptional metabolic profiles reflective of the geological and geochemical
122 characteristics of each individual vent. This study also contributes new *in situ* oxygen data and an
123 expansive metatranscriptomic dataset that enabled differential expression analysis of isotope-
124 enriched transcripts across temperatures within and among vents, and between years. We
125 determined the specific geochemical and thermal conditions under which autotrophic communities
126 and populations are active and identified potential competition amongst these microbial groups for
127 electron acceptors and donors, including oxygen, nitrate, and hydrogen. Overall, these findings
128 expand our knowledge of the distribution and energy acquisition strategies of active subseafloor
129 microbial assemblages in the productive deep-sea hydrothermal vent ecosystem.

130 **RESULTS**

131 Chemical characteristics of all diffuse flow vents are shown in Tables S1 and S2 and
132 include data from both previously published works (see 10, 28) as well as new oxygen data
133 collected with an *in situ* probe (Figs. 1 and S1, Table S3). At all diffuse flow vents, the
134 temperatures ranged from 18.5 to 28.2°C during sampling, the pH was on average ~5.6, and the
135 microbial cell concentrations were the same order of magnitude at each site (1.7-6.8 x 10^5
136 cells/mL) and all an order of magnitude above concentrations in background seawater (Table S1).
137 However, there were clear differences in the diffuse fluid chemical composition among the three
138 vents (Figs. 1 and S1, Tables S1, S2, and S3). At Marker 113 and 33, NO_3^- and H_2 were depleted,

and CH_4 concentrations were elevated. At Anemone, there was evidence for depletion of H_2. Anemone also had the highest H_2S concentrations of all sites. Newly collected oxygen data showed that all the venting sites were depleted relative to near-bottom seawater in the Axial caldera (31 µmol/kg, +/- 2µmol/kg, n=24). Linear regressions of *in situ* O_2 against temperature indicate oxygen behaves differently at each site, with zero O_2 predicted to occur at 33°C for Marker 113 and at 52°C for Marker 33; at Anemone, regression extrapolates to zero O_2 at >100°C (Fig. 1).

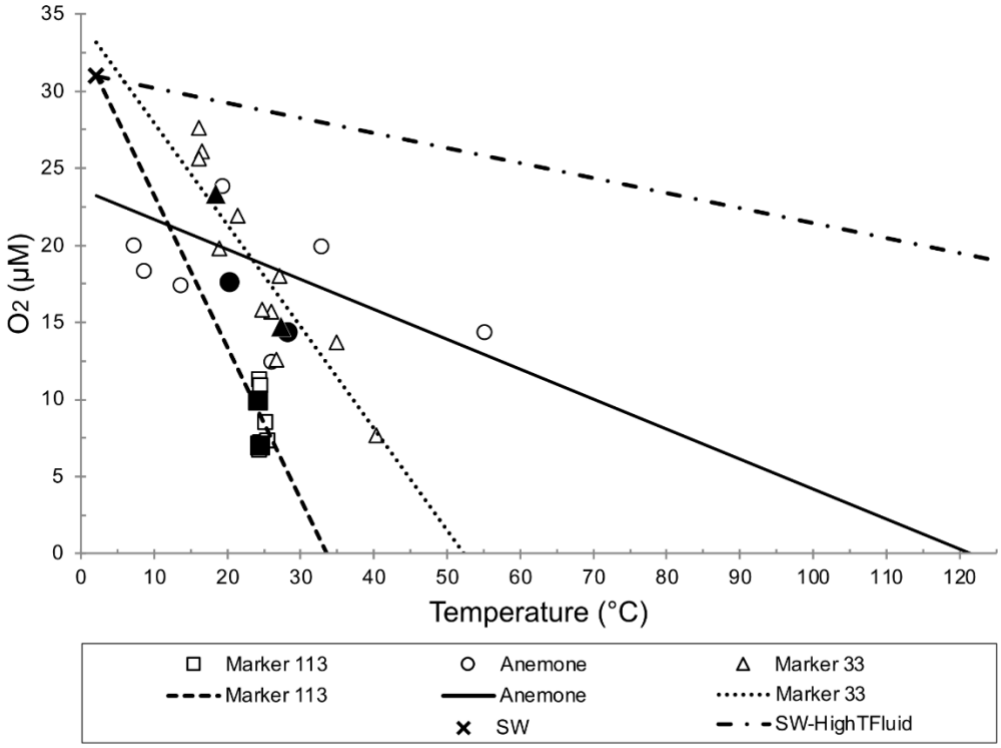

Figure 1. *In situ* oxygen versus temperature for diffuse vents sampled for this study. Near-bottom seawater averages 31 µmol/kg (+/- 2.2) O_2. Linear regression lines are drawn for each of the three vent sites for the two years sampled, including the ambient seawater point in the regression. The SW-HighTFluid line is between seawater and a hypothetical zero-oxygen end-member at 325°C. Solid data points indicate the exact fluid sampling bag used in the SIP experiment.

153 *RNA-SIP experiments*

154 In total, 15 sets of RNA-SIP experiments were carried out in 2013 and 2014 using fluids
155 collected from Marker 113, Anemone, and Marker 33 (Tables 1, S4, and S5). Six of these
156 experiments included two timepoints (Table 1). All 15 RNA-SIP experiments showed a heavier
157 buoyant density peak of RNA in the ^{13}C-labeled experiment compared to the ^{12}C-labeled control,
158 indicating uptake of labeled bicarbonate into RNA (Figs. S3-S5). The highest RNA concentration
159 was chosen from the ^{12}C-light and ^{13}C-heavy peaks for sequencing. If the experiment had two
160 RNA peaks, the two peak fractions were pooled together and sequenced as one sample (Marker
161 113 at 30°C and 80°C, Figs. S3C and S5C). For experiments that had two time points, the ^{12}C-
162 light and ^{13}C-heavy peaks from both time points were sequenced separately. Corresponding ^{13}C-
163 light and ^{12}C-heavy fractions were also sequenced as additional controls, but given their very low
164 RNA concentrations, the sequencing results were not always successful, and these data were not
165 included in any subsequent analyses.

166 Including technical sequencing replicates, there were 84 total metatranscriptomes (44 ^{13}C-
167 heavy and ^{12}C-light, 34 ^{13}C-light and ^{12}C-heavy RNA-SIP experimental metatranscriptomes, and
168 six metatranscriptomes from the *in situ* unmanipulated vent fluid; Table S4) included in this study,
169 totaling over a billion high-quality reads from paired-end Illumina sequencing. Real-time
170 quantitative Reverse Transcription Polymerase Chain Reaction (qRT-PCR) was subsequently
171 carried out to normalize data across experiments using 16S rRNA copies, as shown in Figures S3-
172 S5 (29, 30). In most cases, the highest concentration of RNA corresponded to the highest rRNA
173 copy number.

174 Results from the ^{13}C-heavy RNA-SIP metatranscriptomes are presented as ^{13}C-enriched
175 transcripts throughout the manuscript to distinguish these results from the metatranscriptomes of

176 unmanipulated diffuse fluids. As described in the Methods and Supplementary Methods, the ^{13}C-
177 enriched fraction of the RNA-SIP metatranscriptomes was annotated and compared with the paired
178 metagenome and metatranscriptome generated from unmanipulated diffuse fluids that were
179 filtered and fixed on the seafloor. This comparison enabled both annotation and interpretation of
180 experimental results and ensured results were representative of the native hydrothermal vent
181 microbial community.
182
183 **Table 1**. All RNA-SIP experiments, showing vent name, year, temperature of experiment, and time points
184 collected during incubation.

Vent	**Year**	**30 °C**	**55 °C**	**80 °C**
Marker 113	2013	36 hr	36 hr	18 hr*
Marker 113	2014	n.d.	18 hr, 36 hr	9 hr
Anemone	2013	n.d.	n.d.	18 hr*
Anemone	2014	24 hr, 36 hr	18 hr, 36 hr	18 hr
Marker 33	2013	36 hr	36 hr	36 hr
Marker 33	2014	24 hr, 36 hr	18 hr, 36 hr	9 hr, 18 hr

n.d. = no data; * = 1 L LVWS sample

185 *Taxonomic composition of unmanipulated fluids and ^{13}C-enriched fraction of RNA-SIP*
186 *experiment microbial communities*
187 The unmanipulated fluid metatranscriptomes represent the taxa with detectable transcripts at
188 the instant of sampling via filtration and immediate RNALater fixation on the seafloor. The
189 taxonomy of *in situ* active microbial community members as well as those in the ^{13}C-enriched
190 fraction of RNA-SIP experiments was acquired by mapping non-rRNA transcripts to

191 taxonomically classified metagenomic contigs and then normalizing the genera in each sample to
192 100% (Fig. 2A-D). The taxonomy of the unmanipulated fluids was compared to both the ^{12}C-light
193 and ^{13}C-enriched RNA-SIP taxonomy, and in all but one experiment, the taxonomies of the ^{12}C-
194 light and ^{13}C-enriched fractions of the RNA-SIP metatranscriptomes were comparable (Fig. S6).
195 Therefore, results throughout this study will focus only on the ^{13}C-enriched fraction
196 metatranscriptomes, as they represent the population of isotope-enriched (active) microbes (Fig.
197 2).

198 All genera active at 30°C in the ^{13}C-enriched RNA-SIP metatranscriptomes were also
199 identified in the unmanipulated fluid metatranscriptomes (Fig. 2A). Across all three sites at 30°C,
200 Campylobacterota made up the majority of the active community. *Sulfurimonas* transcripts were
201 observed at all three vents but were most abundant at Marker 113 (52%) (Fig. 2B). Transcripts of
202 *Cetia* (16.8-33.2%) and *Caminibacter* (12.5-22.2%) were found only in the ^{13}C-enriched fraction
203 of RNA-SIP experiments from Anemone. At Marker 33, transcripts belonging to *Hydrogenimonas*
204 (34.3%) were more abundant compared to the other vents.

205 Like the 30°C experiments, all genera active at 55°C in the ^{13}C-enriched fraction of the
206 RNA-SIP metatranscriptomes were also identified in the unmanipulated fluid metatranscriptomes
207 (Fig. 2A). Across all three sites at 55°C, the major differences in taxonomy compared to the 30°C
208 ^{13}C-enriched fraction of the RNA-SIP experiments, was a shift to higher relative abundances of
209 transcripts from *Cetia, Caminibacter, Nautilia,* and *Hydrogenimonas* (Fig. 2C). These taxa
210 dominated experiments from Marker 113 and Marker 33. However, in 2013, transcripts from
211 thermophilic methanogens were detected in addition to Campylobacterota. *Methanothermococcus*
212 comprised 17.3% and 18.6% of the 2013 ^{13}C-enriched fraction of community transcripts at Marker
213 113 and Marker 33, respectively, but were completely absent at Anemone in 2014.

214 Unlike at 30°C and 55°C, where Campylobacterota were abundant in both SIP experiments
215 and unmanipulated fluids, many ^{13}C-enriched active taxa at 80°C were in low abundance in the
216 unmanipulated fluids (Fig. 2A), including those from the Aquificota and *Methanotorris* at Marker
217 113, *Phorcysia* at Anemone, and *Thermovibrio* at Marker 33. The major differences in taxonomy
218 in the ^{13}C-enriched fraction of 80°C RNA-SIP metatransciptomes across sites included a higher
219 abundance of methanogenic groups at Marker 113 and 33, the presence of *Aquifex* only at
220 Anemone, and persistent detection of *Desulfurobacterium* and *Thermovibrio* at all sites and years
221 (Fig. 2D).
222

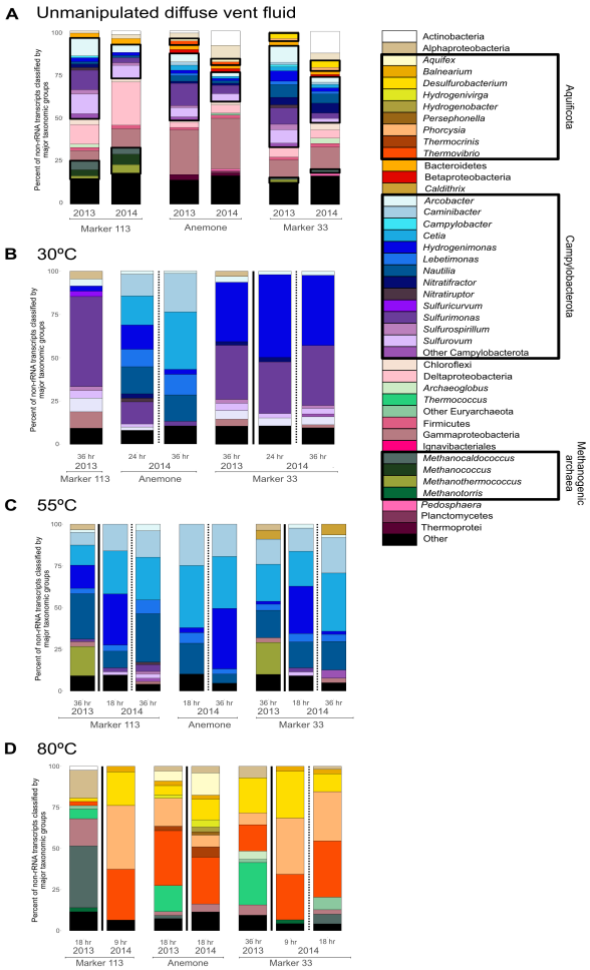

Figure 2. Relative abundance of major taxonomic groups of **A**. Annotated non-rRNA transcripts from unmanipulated fluid metatranscriptomes and annotated non-rRNA transcripts from the ^{13}C-enriched fraction of RNA-SIP experiments at **B**. 30°C, **C**. 55°C, and **D**. 80°C. Black boxes indicate the main autotrophic taxonomic groups recovered from the ^{13}C-enriched fraction of RNA-SIP metatranscriptomes and are drawn onto 2**A** to show how these taxa make up a small proportion of the unmanipulated fluid metatranscriptome to then become the key autotrophs in the ^{13}C-enriched fraction of RNA-SIP metatranscriptomes in 2**B-D.**

Metagenome assembled genomes (MAGs)

233 Binning of the co-assembly of all unmanipulated diffuse fluid, background, and plume
234 metagenomes from Fortunato *et al*. (2018) resulted in 391 bins, with 120 MAGs remaining after
235 filtering for quality (completeness ≥70%, contamination ≤10% based on the presence of single
236 copy bacterial and archaeal marker genes) (10, Table S6). For a phylogenetic tree of the 120
237 quality-filtered MAGs, see Figure S7. After further filtering these MAGs to remove heterotrophs
238 and those only present in the plume, background, or 2015 metagenomes, 25 MAGs remained. The
239 final 11 MAGs were selected based on having >4% of their coding genome expressed [length of
240 expressed genes(bp)/genome length (bp)] in any individual RNA-SIP ^{13}C-enriched fraction (Fig.
241 3, Tables S6 and S7). The taxonomic composition of the highly transcribed MAGs aligned with
242 ORF-based transcript assignments (Figs. 2 and 3), including groups primarily from the Aquificota,
243 Campylobacterota, and methanogens.

244 Both Marker 113 and Marker 33 had *Sulfurimonas* populations (bin 41) transcribed at 30°C
245 (Fig. 3), corresponding to the higher abundance of *Sulfurimonas* transcripts observed at these vents
246 (Fig. 2). Two MAGs classified as *Hydrogenimonas* (bins 102 and 104) were transcribed across
247 different temperatures and vents. Bin 102 was transcribed only at Marker 33 at 30°C, but at 55°C,
248 this bin was transcribed at all vents in at least one timepoint. Bin 104 transcripts, however, were
249 observed only at 30°C at Anemone. Nautiliaceae bin 340 transcripts were ubiquitous at 55°C at all
250 sites and years. *Methanothermococcus* bin 335 transcripts were found at only Marker 113 and
251 Marker 33 at 55°C in 2013, while no methanogen populations were transcribed at Anemone (Figs.
252 2 and 3).

253 In general, MAGs expressed a higher proportion of their coding genomes in the 80°C
254 experiments compared to the other temperatures. *Thermovibrio* MAGs (bin 320 and bin 374) were
255 transcribed across all 80°C experiments, matching the high abundance of the genus in the

transcripts at all vents (Figs. 2 and 3). The Desulfurobacteriaceae (bin 324) was transcribed in 2014 at all sites at 80°C. Aquificales bin 285, however, was restricted to Anemone only (Fig. 3).

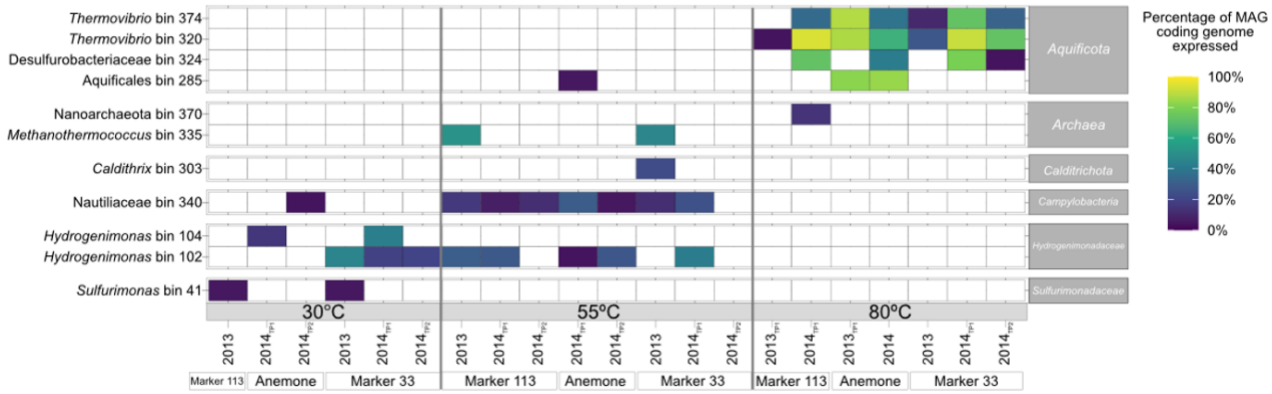

Figure 3. Metagenome Assembled Genomes (MAGs) selected based on having >4% of coding genome expressed in 30, 55 and 80°C ^{13}C-enriched fraction of RNA-SIP experiments. Percent of coding genome expressed = length of expressed genes(bp)/genome length (bp).

Functional attributes of ^{13}C-enriched active autotrophs

To determine how autotrophs in the ^{13}C-enriched fraction of RNA-SIP experiments obtained energy while taking up labeled bicarbonate, we identified transcripts for key genes involved in oxygen, nitrogen, methane, hydrogen, sulfur, and carbon fixation pathways, and compared those to the unmanipulated fluid metatranscriptomes (Fig. 4, Table S8). There were similarities in major metabolic pathways across all sites and samples, but in each year and temperature, the three vent sites differed in magnitude of transcription.

Transcripts for the selected metabolic marker genes were present in most of the unmanipulated fluid metatranscriptomes (Fig. 4), whereas some genes were transcribed in the ^{13}C-enriched fraction of the RNA-SIP metatranscriptomes only at certain temperatures and vents,

274 reflecting specific metabolisms being carried out by distinct subseafloor autotrophic populations
275 under different temperature regimes. We also examined the 30 most abundant transcripts at each
276 RNA-SIP experimental temperature (Fig. S8), some of which were metabolic genes that we note
277 here, while other transcripts were related to information processing, replication and repair, and
278 signaling and cellular processes.

279 Aerobic oxidative phosphorylation gene *aa*$_3$-type cytochrome c oxidase (*coxABCD*) and
280 microaerophily gene *cbb*$_3$-type cytochrome c oxidases (*ccoNOPQ*) transcripts were highest in the
281 ^{13}C-enriched fraction of the 30°C RNA-SIP experiments as compared to 55°C and 80°C (Fig. 4).
282 Normalized counts of *ccoNOPQ* peaked at Marker 33 at 30°C in both 2013 and 2014 (7,593–9,608
283 TPM), attributable to taxa *Aliarcobacter*, *Hydrogenimonas*, *Sulfuricurvum*, *Sulfurimonas*, and
284 *Sulfurovum* (Table S9).

285 Genes for nitrate reduction and complete denitrification were highly transcribed in almost
286 all the ^{13}C-enriched fraction of the RNA-SIP metatranscriptomes (Fig. 4). Of those genes, *napA*,
287 periplasmic nitrate reductase, was the most abundant transcript across all conditions. It was also
288 one of the 30 most transcribed genes at 80°C (1,394–15,195 TPM) (Figs. 4 and S8), predominantly
289 in *Phorcysia* and *Thermovibrio* within the Aquificota. Marker 113, and to a lesser extent, Marker
290 33, had transcription of genes for dissimilatory nitrate reduction to ammonia (DNRA; *nirAB* and
291 *nrfA*, TPMs 8,131–16,106), and these transcripts were uniquely attributed to *Sulfurospirillum*
292 (Table S9).

293 Of the six sulfur marker genes selected, *psr* and *phs* are most functional in anaerobic
294 conditions and *sox* in aerobic conditions (31). However, many sulfur metabolism genes can
295 function across diverse oxic conditions, as they catalyze both anaerobic sulfate reduction and the
296 reverse process, sulfur-compound oxidation (32, 33). Anemone had the highest H_2S concentrations

297 (Table S1) as well as transcription of genes related to sulfur metabolism compared to the other two
298 vents (Fig. 4). For example, *sqr* had high transcription at 80°C (up to 9,695 TPM from *Aquifex*,
299 *Hydrogenivirga*, and *Phorcysia*), whereas at both Marker 113 and Marker 33, *sqr* was transcribed
300 only at 30°C and 55°C (Fig. 4). The highest transcription of polysulfide/thiosulfate reductase genes
301 *psrAC* and *phsAC* occurred at 55°C in all experiments, with transcripts reaching 27,947 TPM from
302 *Hydrogenimonas*, *Cetia*, and *Nautilia* (Fig. S8). Although *soxABCDXYZ* transcripts were present
303 in unmanipulated fluids at all three vents, only Marker 33's 2014 ^{13}C-enriched RNA-SIP
304 metatranscriptome at 30°C showed pronounced transcription (6,396 TPM), derived from
305 *Hydrogenimonas*, *Sulfurovum*, and *Sulfurimonas* (Table S9).

306 Methanogenesis genes were transcribed in the unmanipulated fluid samples from Marker
307 113 and Marker 33 but were largely absent at Anemone (Fig. 4). Transcription of methanogenic
308 metabolic genes was highest in the ^{13}C-enriched RNA-SIP metatranscriptomes from Marker 113
309 in 2013 at 55°C and 80°C (up to 56,765 TPM), and Marker 33 at 55°C in 2013 and at 80°C in
310 2014 (up to 47,489 TPM). These transcripts were attributed to *Methanothermococcus* and
311 *Methanococcus* at 55°C and *Methanotorris* and *Methanocaldococcus* at 80°C. Methanogenic
312 genes *hdrA2* and *mcrA* at 55°C and *frhA*, *fwdB*, *fmdB*, and *mcrAC* at 80°C were among the 30 most
313 transcribed genes in these temperatures (Fig. S8).

314 All metatranscriptomes from unmanipulated diffuse vent fluids contained transcripts from
315 selected hydrogenase marker genes (Fig. 4). Notably, throughout all sites and all years, the ^{13}C-
316 enriched transcriptional profiles from 80°C RNA-SIP experiments lacked the quinone-reactive Ni-
317 Fe hydrogenase *hydAB*, responsible for transferring electrons from H_2 to terminal electron
318 acceptors oxygen, nitrate, sulfate, fumarate, and metals (32). Transcripts for *hydAB* in the 30°C
319 and 55°C experiments belonged to diverse Campylobacterota, predominantly *Sulfuricurvum*

320 (22,883 TPM, Table S9), but also *Sulfurimonas*, *Nautilia*, and *Hydrogenimonas.* Other hydrogen
321 metabolic marker genes, such as sulfhydrogenase (*hydABDG*), energy converting (*echABCDEF*)
322 hydrogenase and Ni-Fe hydrogenase (group 1; *hyaABCD*, *hybCDO*), were in higher abundances
323 at 55°C and 80°C compared to 30°C and associated with *Thermococcus* and Phylum Aquificota
324 (Table S9). F_{420}-non-reducing hydrogenase (*mvhADG*, *vhuADG*, *vhcADG*) used by methanogens
325 was primarily at Marker 113 and 33 at 55°C and 80°C. Some of these hydrogenase marker genes
326 were among the top 30 genes transcribed in the respective temperatures in the dataset (Fig. S8).
327 Across all ^{13}C-enriched RNA-SIP metatranscriptomes at 30°C and 55°C, the most
328 transcribed carbon fixation pathway was the reductive tricarboxylic acid (rTCA) cycle (Fig. 4).
329 The key rTCA marker gene, ATP-citrate lyase *aclAB,* was transcribed in all ^{13}C-enriched RNA-
330 SIP metatranscriptomes at 30°C and 55°C, with transcripts attributed to Campylobacterota (Fig.
331 4, Table S9). At 80°C in both years at Anemone and in 2014 at Marker 113 and Marker 33, *aclAB*
332 transcripts were attributed to Aquificota (Fig. 4, Table S9). In fact, eight genes involved in the
333 rTCA/TCA cycles were among the 30 most abundant genes transcribed at each temperature (Fig.
334 S8). At Marker 113 (2013) and Marker 33 (2014; Tables S8 and S9), in experiments at 80°C when
335 methanogens were active, transcripts for the reductive acetyl-coA (Wood-Ljungdahl) pathway
336 were also abundant, including Wood-Ljungdahl pathway genes (*cooS, acsA*) attributed to
337 *Methanocaldococcus*.

Figure 4. Normalized abundance of non-rRNA transcripts annotated in the unmanipulated diffuse fluid metatranscriptomes (”MetaT“) and ^{13}C-enriched fractions of RNA-SIP metatranscriptomes for key marker genes involving oxygen, nitrogen, sulfur, methane, hydrogen, and carbon fixation. Bubble sizes represent the transcripts per million reads (TPM) attributed to each marker gene.

344 *Differential Expression Analysis of ^{13}C-enriched Transcripts*

345 Differential expression analyses using the RNA-SIP ^{13}C-enriched transcriptional profiles
346 were conducted to determine statistical differences in transcription across experimental conditions
347 without bias towards any specific functional annotations. In the absence of an untreated control in
348 our dataset—an inherent feature of our manipulation of natural environmental samples—we used
349 a differential expression framework that does not require an untreated control and instead
350 compares expression profiles to an expected expression baseline calibrated to each comparison of
351 interest (34-38). Comparisons were made across temperatures within each vent, across
352 temperatures among the three different vents, and between years within each vent (see Methods
353 and Supplementary Methods; 34-38). Across all ^{13}C-enriched RNA-SIP metatranscriptomes, 656
354 unique genes were significantly differentially expressed (SDE) 1520 times with an adjusted p-
355 value of <0.05 (Table S10). Only genes with a padj < 10^{-3} and $\log_2$ fold-change ≥ |2| will be
356 discussed.

357 Across temperatures within each vent, the highest number of transcripts were SDE (483
358 unique genes SDE 1030 times, Fig. 5, Table S11). The baseline for this comparison was the
359 average expression of all ^{13}C-enriched RNA-SIP metatranscriptomes (n=21; Table 1). Within
360 Marker 113, annotated transcripts with the greatest differences in expression across temperatures
361 included gene transcripts for hydrogen metabolism, nitrate reduction, and carbon fixation (Fig.
362 5A). At Marker 113, as RNA-SIP experimental temperature increased, the differentially expressed
363 hydrogenase transcripts in the ^{13}C-enriched fraction shifted from quinone-reactive Ni-Fe
364 hydrogenase genes overexpressed at 30°C (*hydB*) and 55°C (*hydAB*) and underexpressed at 80°C
365 (*hydAB*), to Ni-Fe hydrogenase (group 1) genes (*hyaB*, *hybC*) overexpressed at 80°C and

366 underexpressed at 55°C. Transcripts for hydrogenase genes *mvhA*, *vhuA,* and *vhcA*, utilized in
367 methanogenesis, were underexpressed at 30°C.

368 At Anemone, transcribed genes with the greatest differences in expression across
369 temperatures included transcripts related to carbon fixation and hydrogen, methane, nitrogen, and
370 sulfur metabolism (Fig. 5B). At 55°C, transcripts for Calvin-Benson-Bassham (CBB) cycle genes
371 *rbcSL* and *cbbL* were underexpressed. The hydrogen metabolism genes *hydAB*, and *hyaB*, *hybC*
372 followed the same pattern of differential expression as at Marker 113. At all temperatures at
373 Anemone, transcripts for genes involved in oxygen-sensitive methanogenesis (*mvhG*, *vhuG, vhcG;*
374 *frhABCG*, *hdrA2*) were underexpressed. Nitrate reduction gene transcripts (*napABG*) were
375 underexpressed at 80°C, while transcripts for the nitrite reduction gene *nrfC* were overexpressed
376 at 55°C. Finally, sulfur metabolism gene transcripts for polysulfide/thiosulfate reduction (*phsA*,
377 *psrA*) were underexpressed at 80°C and overexpressed at 55°C (Fig 5B).

378 There were more differentially expressed transcripts across temperature within Marker 33
379 than the other vents, reflecting the greater number of metatranscriptomes in the dataset (n=9 ^{13}C-
380 enriched RNA-SIP metatranscriptomes, Table 1). These included transcripts for hydrogen,
381 methane, nitrogen, and sulfur metabolism (Fig 5C). Marker 33 had the same pattern for differential
382 expression of hydrogenases *hydAB* at 55°C and *hyaB* at 80°C as both Marker 113 and Anemone.
383 Transcripts for methanogenesis genes *frhABCG* were underexpressed at 55°C. Marker 33 had the
384 same genes differentially expressed in the same pattern as Anemone for nitrogen and sulfur
385 metabolism.

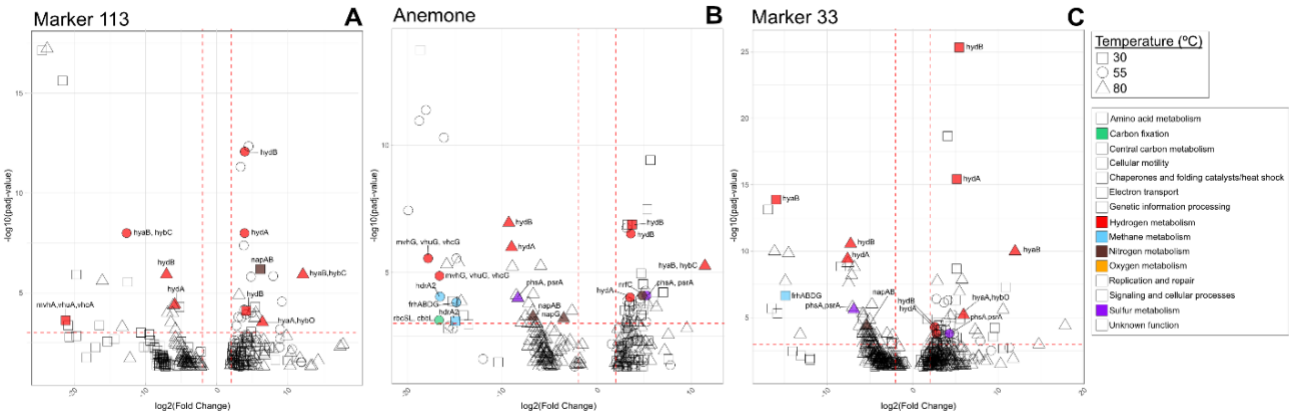

Figure 5. Volcano plots showing the $\log_2$FC (degree of differential expression) across experimental temperatures at each vent **A.** Marker 113, **B.** Anemone, and **C.** Marker 33. Colored and labeled points correspond to genes involved in carbon fixation, hydrogen, methane, nitrogen, oxygen, and sulfur metabolism that had a padj < 10^{-3} and $\log_2$FC > |2| [padj; p-value adjusted for multiple tests using the Benjamini-Hochberg procedure to control the false discovery rate (FDR)].

When comparing across vents by temperature (Fig. S10), 240 transcripts were SDE 329 times, using a baseline expression of normalized transcript counts of all ^{13}C-enriched RNA-SIP metatranscriptomes within each temperature (n=6 for 30°C, n=8 for 55°C, and n=9 for 80°C; Table 1). This comparison revealed SDE transcripts for genes related to hydrogen and nitrogen metabolism. At 30°C, nitrate (*napAB*) and nitrite (*nirA*) reduction gene transcripts were overexpressed only at Marker 113, while nitrate/nitrite (*narGZ*, *nxrA*) reduction gene transcripts were overexpressed at Marker 33 (Fig. S10, Table S12). The greatest number of SDE transcripts was observed at 30°C. None were identified at 55°C, and only three transcripts were SDE in the 80°C experiments.

In a comparison between 2013 and 2014 within each vent, 114 unique genes were SDE 161 times (Fig. S11, Table S13). The baseline expression for this analysis was the same that was used for the across vents by temperature comparison, but the contrast in DESeq2 was switched to

405 time instead of temperature (see Methods). Most SDE gene transcripts were overexpressed at
406 Marker 113 and Marker 33 in 2013, including those for a Wood-Ljungahl pathway carbon fixation
407 gene (*cdhACDE*), methanogenesis hydrogenase genes *mvhA*, *vhuA*, and *vhcA* at Marker 33, and
408 several other methanogenesis genes at both Marker 113 and 33. For Figures with SDE genes coded
409 and annotated by additional general functional categories, see Figures S9, S10 (D-F), and S11 (D-
410 F).

411 **DISCUSSION**

412 In this study, we experimentally manipulated venting fluids to target subseafloor microbes
413 under variable temperature conditions and used stable isotope labeling with inorganic carbon
414 paired with metatranscriptomic sequencing to focus on active autotrophic subseafloor microbes,
415 their metabolic and growth strategies, and their distribution in the subseafloor. While our results
416 broadly corroborated our hypothesis that the subseafloor microbial population structure at each
417 vent and temperature would be distinct, by focusing on only autotrophs at specific temperatures,
418 we also found active, cosmopolitan, subseafloor autotrophs occupying particular thermal niches at
419 all sites, regardless of vent geochemistry or geology. Certain metabolisms and associated lineages
420 such as methanogenic archaea ("specialists") were restricted in distribution, while other
421 metabolisms geared toward hydrogenotrophic sulfur and nitrate utilization and microaerophily
422 ("generalists") were widely distributed in many lineages across a wide temperature range,
423 highlighting metabolic flexibility and functional redundancy across diverse taxonomic groups in
424 this ecosystem. Competition for electron donors like hydrogen and electron acceptors like oxygen
425 was apparent in the data, as shifts in taxonomy and transcription highlighted the conditions under
426 which various microbial groups could dominate. The data suggest that while chemical and physical
427 characteristics at each vent control the energy available for microbial growth—as is the case for

428 methanogenesis and sulfide oxidation—some ubiquitous microbial subseafloor lineages within the
429 young oceanic crust at Axial Seamount have adapted to a broad range of subseafloor chemistries
430 and temperatures and are therefore not restricted in distribution.

431 All ^{13}C-enriched fractions of the RNA-SIP experiments experienced a significant
432 distillation of the taxa present in the unmanipulated fluid metatranscriptomes (Fig. 2). Of note is
433 the reduction or disappearance of *Alpha*-, *Delta*-, and *Gammaproteobacteria*, as well as
434 *Actinobacteria*, groups that comprised up to half of the microbial community in unmanipulated
435 fluids and are common in plume and background seawater samples. The RNA-SIP experiments
436 were amended with hydrogen to re-create energy-rich, warm subseafloor conditions, based on both
437 cultivation experiments from Axial (39) as well as failed RNA-SIP experiments without hydrogen
438 enrichment (8). Along with incubation temperature, this likely explains why these common deep
439 ocean taxa were not heavily represented in the ^{13}C-enriched RNA-SIP metatranscriptomes, as they
440 were either not adapted to these subseafloor conditions or were heterotrophs. Here, we discuss
441 some of the specific patterns of taxonomic distribution, gene expression, and geochemical features
442 across the three vents to determine how the interplay of fluid chemistry, microbial competition,
443 and functional potential results in the autotrophic activity of microbial populations across vents
444 and temperatures.

445 *Restricted methanogenesis, widespread hydrogen utilization*

446 Geochemical profiles of diffuse venting fluids consistently indicated biological hydrogen
447 utilization at all sites and between years, but methane production was only evident at Marker 113
448 and Marker 33 (Fig. S1). These geochemical indicators of biological activity broadly map to the
449 metabolism-focused analyses. ^{13}C-enriched transcripts for methanogenesis, an anaerobic
450 metabolism, were restricted to Marker 113 and 33 (Fig. 4). In addition, the top 30 expressed genes

451 (TPM) at 55°C and 80°C included those related to methanogenesis only at these two vents (Fig.
452 S8). This finding also corresponds to the consistent activity of the singular, high quality
453 *Methanothermococcus* MAG (bin 335) at Marker 113 and 33 (Fig. 3). In contrast, at Anemone,
454 methanogenesis-related ^{13}C-enriched transcripts were absent in the top 30 expressed genes (Figs.
455 4 and S8) and were significantly underexpressed (padj $< 10^{-3}$) compared to other sites. This pattern
456 may result from the oxic regime at Anemone that extends into hotter temperatures relative to the
457 other two vents (Figs. 1 and 4).

458 Whereas methanogenesis was confined to two vents, all sites showed biological utilization
459 of hydrogen, and at Marker 113 and 33, also utilization of nitrate (Fig. S1). ^{13}C-enriched transcripts
460 for hydrogen and nitrate utilization were abundant across all conditions, with overexpression of
461 the periplasmic nitrate reductase genes *napAB* as well as genes for quinone-reactive Ni-Fe
462 hydrogenase (*hydAB*), energy-converting hydrogenase (*echABCDEF*), and Ni-Fe hydrogenase
463 (group 1) (*hyaAB*, *hybBO;* Fig. 4) in the differential expression analysis. Taxonomic assignments
464 of transcripts linked hydrogen oxidation coupled with nitrate reduction to diverse genera, including
465 *Sulfurimonas, Cetia, Hydrogenimonas,* and *Caminibacter* at 30°C; *Cetia, Caminibacter, Nautilia,*
466 *Hydrogenimonas* and those from phylum Aquificota at 55°C; and *Thermovibrio* and
467 *Desulfurobacterium* at 80°C (Fig. 2). Consistent with these transcriptional patterns, diffuse fluid
468 chemistry showed elevated H_2S concentrations at Anemone compared to the other two vents
469 (Tables S1 and S2), correlating with high transcription of polysulfide/thiosulfate reduction genes
470 *psrAC* and *phsAC* (up to 14,000 TPM) in tandem with hydrogen oxidation (Fig. 4). Taxa
471 expressing both *psrAC* and *phsAC* along with quinone-reactive Ni-Fe hydrogenase genes (*hydAB*)
472 at Anemone included *Cetia, Nautilia*, and *Hydrogenimonas*; the latter is known to utilize oxygen
473 as a terminal electron acceptor (41).

474 *Cosmopolitan populations function as subseafloor generalists*

475 Within each year, there were MAGs active in all vents in at least one time point:
476 *Hydrogenimonas* bin 102 (at 55°C in 2014), Nautiliaceae bin 340 (at 55°C in 2013 and 2014),
477 *Thermovibrio* bin 320 (at 80°C 2013 and 2014), and Desulfurobacteriaceae bin 324 (at 80°C in
478 2014). The recurrence of active MAGs across vents and temperatures indicated that some vents at
479 Axial Seamount host the same populations of microorganisms, agnostic of vent geology (basalt
480 vs. sulfides) or geochemistry (Fig. 3). Previous studies (e.g. 9-10, 16, 42) determined that
481 established subseafloor microbial communities are mostly restricted by local vent fluid
482 geochemistry and physical structuring of the site. For example, Fortunato *et al*. (2018) showed
483 MAGs from unmanipulated fluid identified as mesophilic and thermophilic methanogens were
484 restricted mainly to Marker 113 and not Marker 33 or Anemone. This result is connected to both
485 vent chemistry (hydrogen, methane concentrations) and physical mixing, allowing for a more
486 stable subseafloor community at Marker 113 compared to other vents (10). However, our results
487 show this may not be true for all lineages at the population level. Our data reveal that some
488 cosmopolitan taxa are capable of colonizing a wide range of environmental niches, functioning as
489 ecosystem generalists, while lineages restricted in distribution, such as methanogens, serve as an
490 example of ecosystem specialists.

491 The cosmopolitan taxa *Hydrogenimonas* and Nautiliaceae, recovered in 30°C and 55°C
492 experiments, are capable of hydrogenotrophic sulfur and nitrate reduction and are efficient
493 hydrogen oxidizers (43, 44). For example, a study done by Nishimura *et al*. (2010) found that
494 hydrogenases purified from the vent-endemic *Hydrogenimonas thermophila* were
495 phylogenetically related to pathogenic Campylobacterota, known to have high hydrogen oxidation
496 activity (43). Like *Hydrogenimonas, Nautilia profundicola*, another vent-endemic organism, was

497 found to have multiple operons for hydrogenases, including one H_2-sensing (Group 2), two H_2-
498 uptake (Group 1), and three H_2-evolving (Group 4) hydrogenases in their genome. Consistent with
499 the findings from cultured representatives of *Hydrogenimonas* and *Nautilia* that highlight
500 flexibility encoded in their genomes for hydrogen utilization (44), our MAG analyses indicated
501 that bins taxonomically assigned to these genera transcribed three of the four hydrogen marker
502 genes at 55°C, including quinone-reactive Ni-Fe hydrogenase (*hydAB*), Ni-Fe hydrogenase (group
503 1) (*hyaABCD, hybCDO)*, and energy converting hydrogenase (*echABCDEF*; Table S14),
504 indicating the hydrogenase genes were functionally active in these populations.

505 Transcripts for hydrogenases were also detected at 80°C at both the community level and
506 in the ubiquitous Aquificota MAGs, supporting the prevalence and importance of hydrogen
507 oxidation in taxa from this phylum. Transcripts for three hydrogenase marker genes, Ni-Fe
508 hydrogenase (group 1) (*hyaABCD*, *hybCDO*), energy-converting hydrogenase (*echABCDEF*), and
509 sulfhydrogenase, were attributed to both *Desulfurobacterium* and *Thermovibrio* (Figs. 2 and 4,
510 Table S9). Desulfurobacteriaceae bin 324 was present at all vents in 2014 and was found to
511 transcribe the hydrogenase maturation gene *hypF* (Table S14). *Thermovibrio* bin 374, found at all
512 vents in 2013 and 2014, transcribed numerous hydrogenase genes, including an F_{420}-non-reducing
513 hydrogenase gene, hydrogenase maturation gene *hypF,* hydrogenase expression/formation genes
514 *hypED*, and multiple sulfhydrogenase subunits (Table S14). The diversity and versatility of these
515 hydrogenase genes may enable these taxa to grow and survive across vents with different
516 chemistries, leading to the cosmopolitan nature of these populations.

517 *Methanogens and Aquificota compete for hydrogen in subseafloor*

518 Hydrogen is also utilized by hydrogenotrophic methanogens at these vents, and
519 competition for hydrogen among methanogens and the cosmopolitan, hydrogenotrophic sulfur and

520 nitrate reducers of the Aquificota likely occurs in the subseafloor at temperatures >50°C (45-47).
521 Methanogenic growth may be inhibited by growth of these other groups by bringing localized H_2
522 concentrations to a partial pressure below which methanogenesis can occur (48-50). Cultivation
523 experiments showed that *Desulfurobacterium* strain HR11 has a lower H_2 requirement and lower
524 K_s than *Methanocaldococcus* (30 μM vs. 67 μM; 39, 46, 47). In co-culture experiments with
525 *Methanothermococcus thermolithotrophicus* (T_{opt} 65°C), *Methanocaldococcus jannaschii* (T_{opt}
526 82°C), and *Desulfurobacterium thermolithotrophum* (T_{opt} 72°C), Kubik and Holden (2024) found
527 that *D. thermolithotrophum* outcompeted both methanogens at high and low hydrogen
528 concentrations when grown at a 1:1 ratio of initial inoculum (45). However, when *M.*
529 *thermolithotrophicus* was grown at a ratio of 10:1 with *D. thermolithotrophum*, the methanogen
530 outcompeted the bacterium, suggesting the conditions under which methanogens can successfully
531 establish first and grow in larger numbers, as observed in the 55°C experiments at Markers 113
532 and 33, where methanogens were in higher abundance.

533 An additional factor that can influence the distribution and metabolic strategies of
534 hydrogen-utilizing microbes are physical characteristics of the hydrothermal vents. Building off a
535 reactive transport model developed to examine thermophilic versus hyperthermophilic
536 methanogen growth at Axial vents (28), Kubik and Holden expanded the model with additional
537 hydrogenotrophic autotrophs and determined that when the residence time of subseafloor fluids
538 was long, methanogens dominated, but when fluids had shorter residence times, Aquificota
539 dominated. Lower temperatures combined with longer residence times also favored thermophilic
540 methanogenic growth (45). Taken together, our results support these cultivation and modeling
541 studies and show that in the natural world, methanogens require more specific physicochemical
542 conditions for successful growth, thus limiting their distribution, whereas diverse Aquificota and

543 Campylobacterota are more metabolically flexible and less dependent on geochemistry
544 constrained by fluid residence times, enabling a more cosmopolitan distribution. Anemone's close
545 (<1 m) proximity to a high temperature (~300°C) end-member may create short subseafloor fluid
546 residence times; in contrast, Marker 113 and Marker 33 are located farther (~750 m) from a high-
547 temperature venting source, supporting longer fluid residence times, and thus methanogens (28).
548 Our linked geochemical and meta-omics results suggest that the distribution of some subseafloor
549 microbes may be determined by both a microbe's efficiency and genetic regulation of hydrogen
550 utilization as well as the interspecies relationships, chemistry, residence time, and temperature of
551 the subseafloor venting fluids.

552 *Temperature-dependent oxygen regimes structure active autotrophic communities*

553 The novel *in situ* oxygen sensor data enabled new insights into the important role of oxygen
554 as a terminal electron acceptor for subseafloor microbial metabolisms across temperatures and
555 vent locations. Microbial community composition changed with both temperature and site, with
556 Campylobacterota dominating all ^{13}C-enriched RNA-SIP metatranscriptomes up to 80°C. At
557 30°C, ORF-based transcript analysis attributed a substantial proportion of transcripts to
558 *Sulfurimonas* at Marker 113 and *Hydrogenimonas* at Marker 33 (Fig. S12). These results
559 correspond to local oxygen availability: although H_2 concentrations were comparable across these
560 two sites, oxygen-temperature trends predicted anoxia at temperatures above 55°C at both Marker
561 113 and Marker 33 (Fig. 1).

562 At Marker 113, oxygen concentrations were the lowest of all three vents (7.0 μM in 2013,
563 9.9 μM in 2014, Fig. 1, Table S1). While fluid residence times and flow rate impact oxygenation,
564 Marker 113's comparatively low oxygen concentrations may be in part due to *Sulfurimonas* O_2
565 consumption. In the 30°C expression profiles of Marker 113 and Anemone, *Sulfurimonas*

566 transcribed only the cytochrome c oxidase gene, *cbb*$_3$-type (*ccoNOPQ*) and no other genes for
567 alternative electron acceptors, suggestive of a metabolism of oxygen reduction and hydrogen
568 oxidation (Figs. 4 and S12, Table S9). The absence of *Hydrogenimonas* metabolic transcripts and
569 the dominance of *Sulfurimonas* in transcriptional profiles at Marker 113 at 30°C, suggest that
570 microaerophilic *Hydrogenimonas* was limited by low O_2 and/or competition with *Sulfurimonas*.
571 By contrast, the metabolic versatility and higher growth optimum of *Hydrogenimonas* likely
572 support its activity at higher temperatures, where it can utilize alternative electron acceptors (51).

573 At Marker 33, *Sulfurimonas* and *Hydrogenimonas* were recovered in equivalent
574 proportions at 30°C. Here, the persistence of oxygen up to 52°C, closer to the growth optimum of
575 *Hydrogenimonas*, may have allowed both taxa to utilize oxygen at higher temperatures at this site
576 (Fig. 1, Table S3). However, these sustained oxygen concentrations may also inhibit colonization
577 by taxa with similar metabolisms, higher optimum growth temperatures, but lower oxygen
578 tolerance, such as *Caminibacter, Cetia, Lebetimonas*, and *Nautilia*.

579 Beyond the low-temperature patterns, oxygen availability at high temperatures influenced
580 the functional profiles in 80°C incubations at each site. Linear regression modeling showed that
581 oxygen is depleted at 33°C at Marker 113 and 52°C at Marker 33 but persists to at least 100°C at
582 Anemone (Fig. 1). These oxygen models align with the transcript data, as the presence of oxygen
583 at high temperatures at Anemone likely enabled some taxonomic groups to continue utilizing
584 oxygen for microaerophilic sulfide oxidation in 80°C experiments. This result was supported by
585 the transcription of sulfide:quinone oxidoreductase (*sqr*) gene for sulfide oxidation attributed to
586 *Aquifex*, *Hydrogenivirga*, and *Phorcysia*. However, at Marker 113 and Marker 33, the gene for
587 this oxygen-dependent enzyme for autotrophy (40) was not expressed above 55°C, reflecting
588 oxygen depletion at lower temperatures and a shift to alternative electron acceptors such as nitrate.

Conclusions

This study identified subseafloor microbial primary producers at three spatially separated diffuse vents over two years at Axial Seamount and enabled a granular view of the autotrophic microbes at the base of the deep-sea hydrothermal vent ecosystem. The active autotrophs vary among vents, demonstrating that vent geology, fluid chemistry, and flow path shape the geochemical environments and active metabolisms observed. This dynamic interplay between microbial metabolism and vent fluid chemistry not only influences the community structure but also determines which groups dominate under varying environmental conditions. Hydrogen and oxygen availability and utilization is a key control for the establishment of autotrophs, with competition between autotrophic sulfur-reducing taxa and methanogens for hydrogen evident. These interactions underscore the complex ecological networks at hydrothermal vents, where microbial communities not only adapt to but also actively shape their environment through metabolic exchanges and niche differentiation.

MATERIALS AND METHODS

Sample collection

Axial Seamount (Fig. S13) samples were collected using ROVs ROPOS and JASON aboard the *R/V Falkor* and *R/V Thompson* in September 2013 and *R/V Brown* in August 2014 (8, 10). Hydrothermal plume water from 42 m above Anemone (N 45.9335667, W 130.013667) and ambient seawater at 1500 m depth (N 46.27389, W 129.79548) were also collected using a Seabird SBE911 CTD equipped with 10 L Niskin bottles in 2015 aboard the *R/V Thompson*, 5-months post-eruption at Axial Seamount. Water was transferred from Niskin bottles into expandable plastic containers, and 3 L was filtered through 0.22 µm Sterivex filters (Millipore, Billerica, MA, USA) for metagenomic sequencing only.

612 The Hydrothermal Fluid and Particle Sampler (HFPS; 27) and Large Volume Water
613 Sampler (LVWS; 54) were used to collect fluids at ~2 cm above the seafloor. The coordinates for
614 each vent are Marker 113: N 45.9227, W 129.9882; Anemone: N 45.9332, W 130.0137; Marker
615 33: N 45.9332, W 129.9822. Temperature was monitored while drawing fluids using an integrated
616 temperature sensor that was present on both samplers. For sampling with the HFPS and LVWS, a
617 4 L capacity acid-washed Tedlar bag or a 5 L acid-washed plastic carboy, respectively, was used
618 to collect fluids for RNA-SIP experiments as described in (8). DNA and RNA from diffuse fluids
619 for metagenomic (2013-2015) and metatranscriptomic (2013 and 2014) sequencing were
620 concurrently collected using the HFPS at a rate of 100–150 mL min^{-1} through a 0.22 µm, 47 mm
621 GWSP filter (Millipore) on the seafloor for a total volume of 3 L. All filters were preserved *in situ*
622 with RNALater (Ambion, Grand Island, NY, USA) as described in Fortunato *et al*. (2018) (10).
623 RNA-SIP experiments are reported here only from 2013 and 2014, since there were too few
624 samples from 2015 to include in the analysis, though the unmanipulated diffuse fluid metagenomes
625 were included in the assemblies to provide more phylogenetic and functional coverage
626 representative of the Axial diffuse fluid microbial community.

627 Hydrothermal fluid samples were collected with the Hydrothermal Fluid and Particle
628 Sampler (HFPS) following procedures described in (27). Vent fluid samples were analyzed on
629 board for pH, total H_2S, and dissolved methane and hydrogen. Magnesium and nitrate were
630 analyzed on shore. With the exception of oxygen data, these chemical data were previously
631 reported in (10) and used for methanogen modeling in (28). For this study, HFPS included an
632 oxygen optode (SeaBird SBE 63) capable of measuring oxygen concentration in fluids up to a
633 maximum of 40°C. Temperature was monitored at the sample intake, near the sensor block, and
634 inside the oxygen sensor housing. Oxygen measurements were made just before or after collecting

fluid samples, with the intake in the same position to replicate collected water samples. Water was pulled from the titanium/Teflon sampling manifold through the sensor, with some cooling taking place along the flow path. The SBE63 optode does not require a constant flow rate, does not consume oxygen, and can make measurements when flow is stopped. The SBE63 sends 1 Hz serial data, which is received by the HFPS on-board computer. Oxygen concentration is calculated using the temperature measured in the sensor housing, the ambient pressure and salinity (derived from ROV sensors and input manually to the software), and the factory calibration, which covers a temperature range from 2°C to 30°C. All the measurements for this study had temperatures at the sensor within the calibration range. Over the 2013-2015 period of this study, the average oxygen concentration of near-bottom seawater within the caldera, where all diffuse vents for this study are located, was 31 µmol/kg (+/- 2µmol/kg, n=24, Fig 1, Table S2). Oxygen increases significantly with increasing depth at Axial Seamount, where the summit is below the oxygen minimum.

RNA-SIP experimental procedures

Carboys and Tedlar bags were recovered from the ROV and brought to the shipboard lab, where filling into evacuated bottles began immediately. Both were kept at ambient temperature during filling and remained sealed to minimize oxygen exposure, although some likely occurred. The Tedlar bag was housed in a water filled plastic cylinder for collection. As the bag was emptied during bottle filling, additional water was pumped into the cylinder to keep pressure on the bag and minimize outgassing. The time between ROV recovery and experimental set-up was less than 1 hour. For LVWS samples in 2013, fluid from carboys was pumped using a peristaltic pump into evacuated 1 L Pyrex bottles with air-tight butyl stoppers to a volume of 1060 mL. For all other samples in 2013 and 2014, fluid was pumped using a peristaltic pump from the sampling bags or carboys into evacuated 500 mL Pyrex bottles with air-tight butyl stoppers to a volume of 530 mL.

658 Due to limitations in the amount of fluid able to be collected (4 to 5 L), no biological replicates
659 were conducted. During filling, steps were taken to minimize introduction of oxygen and
660 outgassing of fluid. Prior to filling, ^{13}C-labeled sodium bicarbonate (Cambridge Isotope
661 Laboratories, Tewksbury, MA, USA) for the experimental condition or ^{12}C-labeled sodium
662 bicarbonate (Sigma, St. Louis, MO, USA) for the control condition was added to each bottle to a
663 final concentration of 10 mM over background. After filling, the pH of each bottle was measured
664 using pH paper and then adjusted to vent fluid pH (<6.5) by adding 1–2.5 mL of 10% HCl. The
665 headspace was filled with pure H_2 gas using a syringe in the quantity of 20 mL (1698 μmol/kg) for
666 each 500 mL bottle and 60 mL (2547 μmol/kg) for the 1L bottles. ^{12}C- and ^{13}C-bicarbonate
667 amended bottles were each incubated at 30, 55, and 80°C for various times as shown in Table 1 in
668 the main text. Incubation times were chosen to ensure incorporation of the labeled bicarbonate and
669 to minimize cross-feeding, as initially determined in Fortunato and Huber (2016). However, after
670 observation of cross-feeding in these initial experiments, timepoints were added and incubation
671 times reduced for further RNA-SIP experiments. After incubation, the fluid in each bottle was
672 filtered through 0.22 μm Sterivex filters (Millipore). Filtration was completed in less than 30 min,
673 and Sterivex filters were immediately preserved in RNALater (Ambion) and frozen at −80°C.
674 RNA from SIP experiments was extracted according to (8) and detailed in the Supplementary
675 Methods. Following RNA extraction and quantification, each RNA-SIP experiment required
676 isopycnic centrifugation to separate the heavy RNA (labeled with ^{13}C—the active autotrophs) from
677 the light RNA (members of the community that did not take up the ^{13}C label, representing the less
678 active members of that community) as described in (8) and the Supplementary Methods.
679 Four metatranscriptomic libraries were constructed for each RNA-SIP experiment: two
680 from the ^{12}C-control (^{12}C-light and ^{12}C-heavy) and two from the ^{13}C-experiment, (^{13}C-light and

681 ^{13}C-heavy) as described in (8) except for four samples: the second timepoints in 2014 of Marker
682 113 at 55°C, Marker 33 at 30°C and 80°C, and the only timepoint at Anemone at 80°C. The ^{12}C-
683 control incubation peak(s) of highest RNA concentration were used to construct the ^{12}C-light
684 library, which represents the natural community. Similarly, the ^{13}C-experiment incubation peak(s)
685 of highest RNA concentration were used to construct the ^{13}C-heavy library, which represents the
686 labeled, active autotrophic community. The other two libraries from each temperature, ^{12}C-heavy
687 and ^{13}C-light, were constructed to act as additional controls but were not taken through full
688 bioinformatic processing. In some cases (denoted in Figs. S3-S5), two RNA fractions were
689 combined for library construction.
690 *Metagenomic bioinformatic analyses*
691 All metagenomic libraries were constructed as described in the Supplementary Methods. There
692 were 11 metagenome samples processed, including metagenomes from all three vent sites in 2015
693 (Table S4; 10). These samples were included to provide a comprehensive functional repertoire in
694 diffuse fluid communities at Axial Seamount (10). A pipeline with code used in metagenomic
695 processing can be found here: https://github.com/corporeal-snow-albatross-
696 5/Axial_Metagenomics. Samples were first trimmed of Illumina adapter sequences using
697 Trimmomatic (v0.32; 55), quality checked using FastQC (v0.11.9; 56), and quality results were
698 aggregated across samples into a single report using MultiQC (v1.12; 57). These initial trimming
699 and quality control steps were done using the qc-trim Snakemake pipeline
700 (https://github.com/shu251/qc-trim). The separate forward reads and separate reverse reads were
701 combined using the cat (concatenate) command in Unix and then concatenated forward and reverse
702 read files were combined using the fq2fa (v1.1.3) function within the IDBA_UD assembler (58;
703 https://github.com/loneknightpy/idba). Each of the metagenomes were assembled using

704 IDBA_UD (v1.1.3), using a max kmer size of 120 (58; https://github.com/loneknightpy/idba).
705 Contig and scaffold quality was evaluated using MetaQUAST (v5.0.2; 59), and the best assembly
706 given steps of 20 from kmer lengths of 20-120 was chosen for further analysis. Each metagenome
707 was submitted to the DOE Joint Genome Institute's Integrated Microbial Genome Expert Review
708 (IMG/ER) for annotation. IMG/ER JGI GOLD Analysis Project ID numbers can be found in Table
709 S4. Open reading frame (ORF) information from the IMG/ER annotation was extracted using a
710 python script to create .ffn files from .gff (containing contig and locus identity, start and stop sites
711 of ORFs, and strand information) and .fna files (containing the nucleotide sequence of each ORF).
712 All metagenome .ffn files were then concatenated to make one long, annotated assembly using the
713 cat command in Unix.

714 The ORFs predicted in each metatranscriptomic (mRNA) file were mapped back to the
715 concatenated metagenomic assembly, which was first indexed using the kallisto index function
716 within the pseudoaligner Kallisto prior to mapping (v.0.46.0; 60). Post-mapping, the KEGG
717 Ontology (KO) ID's and the taxonomy of each predicted ORF in the metagenomes were retrieved
718 from IMG/ER. Cutoffs on the minimum requirements of an e-score of 10^{-10}, 30% amino acid
719 identity, and alignment length of 40 amino acids were imposed, as used in (10). Additionally,
720 eukaryote and virus hits were filtered out of the taxonomy file. Before filtering, there were
721 5,432,185 contigs classified as eukaryotes or viruses, and after filtering, the classified contig count
722 was 5,309,746. Therefore only 2.25% of the total contigs were identified as eukaryotes or viruses,
723 meaning most hits belonged to bacteria and archaea. The filtered KO tables of each metagenome
724 were concatenated with each other, and the same was done for the taxonomy tables. The
725 concatenated KO and taxonomy tables were then combined with each other using an inner_join in
726 the R dplyr package (61, 62), based on target_id (predicted ORF).

727 *Metagenome Assembled Genome (MAG) generation and analysis*

728 In addition to an annotated, concatenated assembly, a co-assembly using the quality-
729 filtered and trimmed reads from 11 metagenomic samples was also constructed using MEGAHIT
730 (v1.2.9; 63) with parameters --min-contig-len = 200, --presets = "meta-sensitive". Assembly
731 statistics were checked using MetaQUAST (v5.0.2; 59). The resulting assembly had 2,318,625
732 contigs that were at least 500 bp in length; of those contigs, the N50 = 721 bp and maximum length
733 = 280,659 bp. The co-assembled metagenome (hereafter referred to as the "co-assembly") was
734 annotated through the DOE Joint Genome Institute's Integrated Microbial Genome Expert Review
735 (IMG/ER) pipeline. IMG/ER JGI GOLD Analysis Project ID numbers can be found in Table S4.
736 The resulting gene calls, .gff annotation file, and phylodist taxonomy of contigs, were used as the
737 reference material for the metagenome assembled genomes (MAGs), differential gene expression
738 analyses, taxonomy assessments, and overviews of functional potential versus expression. KEGG
739 Ontology (KO) ID's and the taxonomy of each predicted ORF in the co-assembly were retrieved
740 from IMG/ER. Cutoffs on the minimum requirements of an e-score of 10^{-10}, 30% amino acid
741 identity, and alignment length of 40 amino acids were imposed, as used in (10).

742 MetaBAT2 (v2.15; 64) was used to generate binned contigs. The co-assembly was first
743 indexed using the bwa index within BWA mem (v7.17; 65) and then metagenomes were mapped
744 to the indexed file. The resulting output was processed through Samtools (v1.13; 66). The .sam file
745 generated from mapping was converted to a .bam file using the samtools view function and
746 resulting .bam files were sorted using samtools sort. Prior to binning, depth (also called coverage)
747 files were created for each metagenome and binned with a minimum contig length of 1500 using
748 MetaBAT2. DAS Tool was then used to resolve redundancy among bins and provide an optimized
749 bin set (v1.1.7, 67). Bins were taxonomically classified using GTDB-tk (v2.1.1; 68).

750 We refer to unscreened binning outputs as 'bins.' Bins with >70% completeness and <10%
751 contamination are termed metagenome-assembled genomes (MAGs; Table S5). Genomic binning
752 from all the diffuse fluid metagenomes resulted in 391 bins, and after removing redundant bins
753 using DAS Tool (v1.1.7; 67), 120 MAGs remained with 45 having <10% contamination and being
754 >70% complete (Table S5). The MAGs were further filtered to remove known heterotrophs (based
755 on literature searches) and MAGs solely sourced from the plume, background, or 2015
756 metagenomes. This resulted in 25 MAGs remaining. To further narrow the MAGs to those most
757 active in our samples, we determined the percent expressed coding genome for each bin within
758 each of the RNA-SIP metatranscriptomic samples. The expressed coding genome was calculated
759 as the length of the transcripts recruited to each bin (bp) for each sample, divided by MAG size
760 (bp). The final 11 MAGs were selected based on having >4% of their coding genome expressed in
761 any individual RNA-SIP ^{13}C-enriched metatranscriptome (Fig. 3 in the main text, Table S7).
762

763 *Metatranscriptomic bioinformatic analyses*

764 Metatranscriptomic libraries from unmanipulated fluids were constructed as described in
765 the Supplementary Methods. In total, there were 84 metatranscriptome samples processed: 6
766 metatranscriptomes from unmanipulated fluids at each vent in 2013 and 2014 and 78 RNA-SIP
767 metatranscriptomes (Table S4). A pipeline containing the code used to process metatranscriptomes
768 is located here: https://github.com/corporeal-snow-albatross-5/Axial_Metatranscriptome.
769 Metatranscriptomic sequences were trimmed and quality checked with the same methods and
770 software parameters as the metagenomic sequences. The separate forward reads and separate
771 reverse reads were concatenated using the cat command in Unix and then concatenated forward
772 and reverse read files were combined using Fast Length Adjustment of Short reads (FLASH;
773 v.1.2.11; 69), which is a program used to combine fastq files. The only parameter set was for read
774 length, which was 110 bp. Although metatranscriptome libraries were constructed with selective
775 amplification for mRNA (not rRNA), the SIP metatranscriptomes were not. To separate the rRNA
776 for preliminary taxonomic analyses from the mRNA for downstream processing, SortMeRNA
777 (v4.2.0; 70) was used (Table S5). The SILVA v.132 bacterial and archaeal 16S (id85), 23S (id98),
778 and 5S (id98) databases were used as reference databases to map the rRNA. The rest of the
779 parameters were: --fastx for a fastq output format, --other for mRNA reads that did not map to the
780 databases, --out2, and --pairedout for non-aligned reads. The percentage of reads mapping to rRNA
781 from SortMeRNA can be found in Table S5.

782 Fastq reads from SortMeRNA rRNA output were converted to fasta format using the fq2fa
783 (v.1.1.3) function within IDBA_UD assembler (58; https://github.com/loneknightpy/idba). rRNA
784 taxonomy was classified using mothur classify.seqs function and the SILVA (v.132) 16S rRNA
785 reference database (71). The 5S rRNA database used as one of the reference databases for rRNA

786 mapping in SortMeRNA also contains eukaryotes. As such, the eukaryote hits were removed
787 before further processing. Taxonomy count tables were generated using R (61), and bar plotting
788 for rRNA was done via ggplot2 (72) within tidyverse (73) in R. Resulting plots were only used to
789 compare to ORF transcript taxonomy and are not included in this paper.

790 Fastq mRNA reads were mapped to the indexed concatenated metagenomic assembly using
791 the kallisto quant function within Kallisto (v0.46.0; 60), which also normalized all ORFs that
792 mapped, providing Transcripts Per Million (TPM) values for each ORF. TPM normalizes for both
793 gene length and depth of sequencing, allowing for accurate comparisons between samples (74).
794 Sample names were attached to kallisto output files, then all files were concatenated and tpm values
795 of 0 were removed. This table was then attached to the KO and taxonomy table made from the
796 IMG/ER output using an inner_join in the R dplyr package (61, 62), based on target_id (predicted
797 ORF). 784,486 total ORFs from all samples joined out of 4,027,381 total, which means
798 that 80.521% of ORFs from the concatenated metagenome were unmatched in KO and taxonomy
799 in the metatranscriptomes and SIP metatranscriptomes. There were no eukaryote hits in the ORFs
800 that had a match with both KO and taxonomy. There were only 11 virus hits in these samples of
801 784,486 total ORFs that did have matching KO's and taxonomy. Because few viruses and no
802 eukaryotes were found, they were removed for further processing and to enable comparability
803 between the rRNA and ORF taxonomy. All figures and statistical analyses were completed in R
804 (61).
805

806 *Differential expression analysis*

807 Metatranscriptomic (mRNA) samples from the ^{13}C-enriched fractions of Marker 113,
808 Anemone, and Marker 33 incubations at 30, 55, and 80°C from 2013 and 2014 were pseudoaligned
809 to the indexed co-assembly using kallisto (parameters: --single -l 151 -s 41) (v0.46.0; 60). The
810 kallisto outputs of metatranscriptome pseudocounts were tabulated with the R package tximport
811 (v1.26.1; 36) using a custom annotation database of unique genes collapsed into protein-coding
812 gene representatives. Due to the diversity in metagenomes, the co-assembly annotation contained
813 multiple targets for gene products. To reduce complexity in functional expression analyses,
814 protein-coding genes observed in the co-assembly were indexed into protein families using IMG's
815 highest confidence annotation such as KEGG, COG, pfam, and TIGRFAM. ORFs annotated with
816 only "hypothetical protein" were discarded. The annotation database indexed 2,428,812 genes
817 representing 14,942 unique genes collapsed into protein-coding gene representatives observed in
818 the co-assembly. When referring to genes and proteins in our evaluations of differential functional
819 expression, we are using this consolidated database.

820 Differential expression analyses were conducted in R with DESeq2 (v1.38.3; 34, 35), and
821 code can be found here: https://github.com/corporeal-snow-albatross-
822 5/Axial_Differential_Expression. Our experimental design included three different conditions
823 (vent, temperature, and year) with two or more levels (the possible values each variable can take
824 in the DE statistical model). For vent, there are three levels: Marker 113, Anemone, and Marker
825 33; for temperature there are also three levels: 30°C, 55°C, and 80°C; for year, there are two levels:
826 2013 and 2014. Because the number of samples across conditions was uneven (i.e. the number of
827 RNA-SIP experiments differed between years and across vents and temperatures, Table 2), we
828 implemented methodology for imbalanced designs and multi-group data, as described in Love *et*

829 *al*. (2014b) (35). First, we manually defined contrasts (grouping of samples for each comparison)
830 to account for an imbalance of samples in the DESeq2 model design (37, 38). This allowed for the
831 model to identify differential gene expression without requiring an untreated control. Subsetting
832 the dataset minimized the observed within-group variability caused by unparameterized interaction
833 of variables, thereby reducing stochasticity and improving assessment of significant genes. This
834 permitted us to tailor baseline gene expression for each of the three comparisons: across
835 experimental temperatures within each vent (1030 significantly differentially expressed (SDE)
836 transcripts; Table S11), across vents by temperature (329 SDE transcripts; Table S12), and
837 between 2013 and 2014 within each vent (161 SDE transcripts; Table S13).

838 For temperature comparisons within each vent (i.e. all Anemone experiments at 30, 55, and
839 80°C compared to one another), the baseline expression for genes was the normalized expression
840 of all ^{13}C-enriched metatranscriptomic fractions (n=21; Table 2). For across vent comparisons at
841 a single temperature (i.e. All 30°C experiments across all vents), as well as comparisons between
842 years within each vent (i.e. 2013 Marker 113 80°C incubation compared to 2014 Marker 113 80°C
843 incubation), gene baseline expressions were calculated at each incubation temperature: 6 ^{13}C-
844 enriched metatranscriptomes at 30°C; 8 ^{13}C-enriched metatranscriptomes at 55°C; and 7 ^{13}C-
845 enriched metatranscriptomes at 80°C. Volcano plots show genes with p-values adjusted for
846 multiple test correction using the Benjamini-Hochberg procedure to control the false discovery
847 rate (FDR, 35), with padj < 0.001 and log2 fold-change > |2|; only genes involved in carbon
848 fixation, hydrogen, methane, nitrogen, oxygen, and sulfur metabolism are shown in Figures 6,
849 S10A-C, and S11A-C. Plots with expanded gene function annotations are shown in Figures S9,
850 S10D-F, and S11D-F. For additional details about how the differential expression analysis was
851 conducted, see the Supplementary Methods.

DATA AVAILABILITY

All raw metagenomic and metatranscriptomic read data are publicly available through the Sequence Read Archive (SRA). Metagenomic assemblies are publicly available through JGI GOLD. All accession numbers are located in Table S4.

ACKNOWLEDGEMENTS

This work was funded by the Gordon and Betty Moore Foundation Grant GBMF3297; the NSF Center for Dark Energy Biosphere Investigations (C-DEBI) (OCE-0939564), contribution number TBD, NOAA/PMEL, contribution number TBD; the Joint Institute for the Study of the Atmosphere and Ocean (JISAO) under NOAA Cooperative Agreement NA15OAR4320063, contribution number TBD; and the National Aeronautics and Space Administration (NASA) grant number 80NSSC19K1427.

The NOAA/PMEL supported this work with ship time in 2014 and through funding to the Earth Ocean Interactions group. The 2013 data collected in this study includes work supported by the Schmidt Ocean Institute during cruise FK010–2013 aboard R/V Falkor. The NOAA/PMEL (through funding to the Earth Ocean Interactions group) and GBMF supported field work in 2014 with ship and vehicle time aboard the R/V Brown (RB2014-03). We thank the captains and crews of the *R/V Falkor, R/V Thompson* and *R/V Brown* as well as the outstanding ROV teams of the vehicles *ROPOS*, *SuBastian*, and *JASON*.

Sarah Hu, Connor Scannerton, and Margrethe Serres provided guidance on the analysis and code used to process this dataset, while the Keck Facility at the Josephine Bay Paul Center at the Marine Biological Laboratory provided support for sequencing. Kevin Roe, Noah Lawrence-Slavas, Susan Merle, Andra Bobbit, and William Chadwick provided support at sea.

REFERENCES

875 1. Dick GJ. 2019. The microbiomes of deep-sea hydrothermal vents: distributed globally, shaped
876 locally. *Nat Rev Microbiol* 17:271–283.
877 2. Jannasch HW, Mottl MJ. 1985. Geomicrobiology of deep-sea hydrothermal vents. *Science*
878 229:717–725.
879 3. Summit M, Baross JA. 2001. A novel microbial habitat in the mid-ocean ridge subseafloor.
880 *Proc Natl Acad Sci* 98:2158–2163.
881 4. Reysenbach A-L, Shock E. 2002. Merging genomes with geochemistry in hydrothermal
882 ecosystems. *Science* 296:1077–1082.
883 5. McCollom TM. 2005. Energetic constraints on subsurface biomass production within the
884 igneous ocean crust. *Geochimica et Cosmochimica Acta* 69:A200.
885 6. Huber JA, Holden JF. 2008. Modeling the impact of diffuse vent microorganisms along mid-
886 ocean ridges and flanks. *In* Magma to Microbe: Modeling Hydrothermal Processes at Ocean
887 Spreading centers Jan 1;178:215-31.
888 7. Amend JP, McCollom TM, Hentscher M, Bach W. 2011. Catabolic and anabolic energy for
889 chemolithoautotrophs in deep-sea hydrothermal systems hosted in different rock types.
890 *Geochim Cosmochim Acta* 75:5736–5748.
891 8. Fortunato CS, Huber JA. 2016. Coupled RNA-SIP and metatranscriptomics of active
892 chemolithoautotrophic communities at a deep-sea hydrothermal vent. *ISME J* 10:1925–1938.
893 9. Olins HC, Rogers DR, Preston C, Ussler W 3rd, Pargett D, Jensen S, Roman B, Birch JM,
894 Scholin CA, Haroon MF, Girguis PR. 2017. Co-registered Geochemistry and
895 Metatranscriptomics Reveal Unexpected Distributions of Microbial Activity within a
896 Hydrothermal Vent Field. *Front Microbiol* 8:1042.

10. Fortunato CS, Larson B, Butterfield DA, Huber JA. 2018. Spatially distinct, temporally stable microbial populations mediate biogeochemical cycling at and below the seafloor in hydrothermal vent fluids. *Environ Microbiol* 20:769–784.

11. McNichol J, Stryhanyuk H, Sylva SP, Thomas F, Musat N, Seewald JS, Sievert SM. 2018. Primary productivity below the seafloor at deep-sea hot springs. *Proc Natl Acad Sci* 115:6756–6761.

12. Opatkiewicz AD, Butterfield DA, Baross JA. 2009. Individual hydrothermal vents at Axial Seamount harbor distinct subseafloor microbial communities. *FEMS Microbiol Ecol* 70:413–424.

13. Perner M, Bach W, Hentscher M, Koschinsky A, Garbe-Schönberg D, Streit WR, Strauss H. 2009. Short-term microbial and physico-chemical variability in low-temperature hydrothermal fluids near 5 degrees S on the Mid-Atlantic Ridge. *Environ Microbiol* 11:2526–2541.

14. Perner M, Hansen M, Seifert R, Strauss H, Koschinsky A, Petersen S. 2013. Linking geology, fluid chemistry, and microbial activity of basalt- and ultramafic-hosted deep-sea hydrothermal vent environments. *Geobiology* 11:340–355.

15. Huber JA, Mark Welch DB, Morrison HG, Huse SM, Neal PR, Butterfield DA, Sogin ML. 2007. Microbial population structures in the deep marine biosphere. *Science* 318:97–100.

16. Huber JA, Cantin HV, Huse SM, Welch DBM, Sogin ML, Butterfield DA. 2010. Isolated communities of Epsilonproteobacteria in hydrothermal vent fluids of the Mariana Arc seamounts. *FEMS Microbiol Ecol* 73:538–549.

17. Akerman NH, Butterfield DA, Huber JA. 2013. Phylogenetic diversity and functional gene patterns of sulfur-oxidizing subseafloor Epsilonproteobacteria in diffuse hydrothermal vent fluids. *Front Microbiol* 4:185.

18. Larson BI, Houghton JL, Lowell RP, Farough A, Meile CD. 2015. Subsurface conditions in hydrothermal vents inferred from diffuse flow composition, and models of reaction and transport. *Earth Planet Sci Lett* 424:245–255.

19. Meier D. 2016. PhD Thesis. University of Bremen, Bremen, Germany. Bacterial niche adaptation at hydrothermal vents.

20. Reveillaud J, Reddington E, McDermott J, Algar C, Meyer JL, Sylva S, Seewald J, German CR, Huber JA. 2016. Subseafloor microbial communities in hydrogen-rich vent fluids from hydrothermal systems along the Mid-Cayman Rise. *Environ Microbiol* 18:1970–1987.

21. Galambos D, Anderson RE, Reveillaud J, Huber JA. 2019. Genome-resolved metagenomics and metatranscriptomics reveal niche differentiation in functionally redundant microbial communities at deep-sea hydrothermal vents. *Environ Microbiol* 21:4395–4410.

22. Fullerton H, Smith L, Enriquez A, Butterfield D, Wheat CG, Moyer CL. 2024. Seafloor incubation experiments at deep-sea hydrothermal vents reveal distinct biogeographic signatures of autotrophic communities. *FEMS Microbiol Ecol* 100.

23. Trembath-Reichert E, Butterfield DA, Huber JA. 2019. Active subseafloor microbial communities from Mariana back-arc venting fluids share metabolic strategies across different thermal niches and taxa. *ISME J* 13:2264–2279.

24. Fortunato CS, Butterfield DA, Larson B, Lawrence-Slavas N, Algar CK, Zeigler Allen L, Holden JF, Proskurowski G, Reddington E, Stewart LC, Topçuoğlu BD, Vallino JJ, Huber JA. 2021. Seafloor incubation experiment with deep-sea hydrothermal vent fluid reveals effect of pressure and lag time on autotrophic microbial communities. *Appl Environ Microbiol* 87.

941 25. Lueders T. 2010. Stable isotope probing of hydrocarbon-degraders. p 4011–4026. In Timmis
942 KN (ed), Handbook of Hydrocarbon and Lipid Microbiology. Springer, Berlin.
943 https://doi.org/10.1007/978-3-540-77587-4_312
944 26. Lueders T, Dumont MG, Bradford L, Manefield M. 2016. RNA-stable isotope probing: from
945 carbon flow within key microbiota to targeted transcriptomes. *Curr Opin Biotechnol* 41:83–
946 89.
947 27. Butterfield DA, Roe KK, Lilley MD, Huber JA, Baross JA, Embley RW, Massoth GJ. 2004.
948 Mixing, reaction and microbial activity in the sub-seafloor revealed by temporal and spatial
949 variation in diffuse flow vents at Axial Volcano. *In* The Subseafloor Biosphere at Mid-Ocean
950 Ridges 144:269–289.
951 28. Stewart LC, Algar CK, Fortunato CS, Larson BI, Vallino JJ, Huber JA, Butterfield DA, Holden
952 JF. 2019. Fluid geochemistry, local hydrology, and metabolic activity define methanogen
953 community size and composition in deep-sea hydrothermal vents. *ISME J* 13:1711–1721.
954 29. Glaubitz S, Lueders T, Abraham WR, Jost G, Jürgens K, Labrenz M. 2009. 13C-isotope
955 analyses reveal that chemolithoautotrophic Gamma- and Epsilonproteobacteria feed a
956 microbial food web in a pelagic redoxcline of the central Baltic Sea. *Environ Microbiol*
957 11:326–337. https://doi.org/10.1111/j.1462-2920.2008.01772.x
958 30. Bradford LM, Vestergaard G, Táncsics A, Zhu B, Schloter M, Lueders T. 2018.
959 Transcriptome-stable isotope probing provides targeted functional and taxonomic insights into
960 microaerobic pollutant-degrading aquifer microbiota. *Front Microbiol* 9:2696.
961 https://doi.org/10.3389/fmicb.2018.02696
962 31. Zhou Z, Tran PQ, Cowley ES, Trembath-Reichert E, Anantharaman K. 2024. Diversity and
963 ecology of microbial sulfur metabolism. *Nat Rev Microbiol* 23:122–140.

964 32. Takai K, Campbell BJ, Cary SC, Suzuki M, Oida H, Nunoura T, Hirayama H, Nakagawa S,
965 Suzuki Y, Inagaki F, Horikoshi K. 2005. Enzymatic and genetic characterization of carbon and
966 energy metabolisms by deep-sea hydrothermal chemolithoautotrophic isolates of
967 Epsilonproteobacteria. *Appl Environ Microbiol* 71:7310–7320.
968 33. Nakagawa S, Takai K. 2008. Deep-sea vent chemoautotrophs: diversity, biochemistry and
969 ecological significance: Chemoautotrophy in deep-sea vents. *FEMS Microbiol Ecol* 65:1–14.
970 34. Love MI, Huber W, Anders S. 2014a. Moderated estimation of fold change and dispersion
971 for RNA-seq data with DESeq2. *Genome Biol* 15:550.
972 35. Love MI, Anders S, Huber W. 2014b. Differential analysis of count data–the DESeq2
973 package. *Genome Biol* 15:550. https://doi.org/10.1186/s13059-014-0550-8
974 36. Soneson C, Love MI, Robinson MD. 2015. Differential analyses for RNA-seq: transcript-
975 level estimates improve gene-level inferences. F1000Res 4:1521.
976 https://doi.org/10.12688/f1000research.7563.2
977 37. Tavares H. 2023. DESeq2 contrasts tutorial. GitHub.
978 https://github.com/tavareshugo/tutorial_DESeq2_contrasts/blob/main/DESeq2_contrasts.md
979 (Accessed 20 June 2025).
980 38. Love MI, Huber W, Anders S. 2025. DESeq2: Differential gene expression analysis based on
981 the negative binomial distribution. Bioconductor.
982 https://www.bioconductor.org/packages/devel/bioc/vignettes/DESeq2/inst/doc/DESeq2.html
983 #expanded-model-matrices (Accessed 20 June 2025).
984 39. Ver Eecke HC, Butterfield DA, Huber JA, Lilley MD, Olson EJ, Roe KK, Evans LJ, Merkel
985 AY, Cantin HV, Holden JF. 2012. Hydrogen-limited growth of hyperthermophilic
986 methanogens at deep-sea hydrothermal vents. *Proc Natl Acad Sci* 109:13674–13679.

987 40. Nübel T, Klughammer C, Huber R, Hauska G, Schütz M. 2000. Sulfide:quinone
988 oxidoreductase in membranes of the hyperthermophilic bacterium Aquifex aeolicus (VF5).
989 *Arch Microbiol* 173:233–244.
990 41. Takai K, Nealson KH, Horikoshi K. 2004. Hydrogenimonas thermophila gen. nov., sp. nov.,
991 a novel thermophilic, hydrogen-oxidizing chemolithoautotroph within the epsilon-
992 Proteobacteria, isolated from a black smoker in a Central Indian Ridge hydrothermal field.
993 *Int J Syst Evol Microbiol* 54:25–32.
994 42. Perner M, Hentscher M, Rychlik N, Seifert R, Strauss H, Bach W. 2011. Driving forces behind
995 the biotope structures in two low-temperature hydrothermal venting sites on the southern Mid-
996 Atlantic Ridge: Driving forces behind vent biotopes. *Environ Microbiol Rep* 3:727–737.
997 43. Nishimura H, Kitano Y, Inoue T, Nomura K, Sako Y. 2010. Purification and characterization
998 of membrane-associated hydrogenase from the deep-sea epsilonproteobacterium
999 Hydrogenimonas thermophila. *Biosci Biotechnol Biochem* 74:1624–1630.
1000 44. Campbell BJ, Smith JL, Hanson TE, Klotz MG, Stein LY, Lee CK, Wu D, Robinson JM,
1001 Khouri HM, Eisen JA, Cary SC. 2009. Adaptations to submarine hydrothermal environments
1002 exemplified by the genome of *Nautilia profundicola. PLoS* Genet 5:e1000362.
1003 45. Kubik BC, Holden JF. 2024. Non-thermodynamic factors affect competition between
1004 thermophilic chemolithoautotrophs from deep-sea hydrothermal vents. *Appl Environ*
1005 *Microbiol* 90:e0029224.
1006 46. Stewart LC. 2015. PhD thesis. University of Massachusetts Amherst, Amherst, MA. Energetic
1007 Limitations of Thermophilic Methanogens And Thiosulfate Reducers in The Subsurface
1008 Biosphere at Deep-Sea Hydrothermal Vents.

1009 47. Stewart LC, Llewellyn JG, Butterfield DA, Lilley MD, Holden JF. 2016. Hydrogen and
1010 thiosulfate limits for growth of a thermophilic, autotrophic Desulfurobacterium species from a
1011 deep-sea hydrothermal vent. *Environ Microbiol Rep* 8:196–200.
1012 48. Kristjansson JK, Schönheit P, Thauer RK. 1982. Different K_s values for hydrogen of
1013 methanogenic bacteria and sulfate reducing bacteria: An explanation for the apparent inhibition
1014 of methanogenesis by sulfate. *Arch Microbiol* 131:278–282.
1015 49. Lovley DR, Dwyer DF, Klug MJ. 1982. Kinetic analysis of competition between sulfate
1016 reducers and methanogens for hydrogen in sediments. *Appl Environ Microbiol* 43:1373–1379.
1017 50. Robinson JA, Tiedje JM. 1984. Competition between sulfate-reducing and methanogenic
1018 bacteria for H_2 under resting and growing conditions. *Arch Microbiol* 137:26–32.
1019 51. Takai K, Nealson KH, Horikoshi K. 2004. Hydrogenimonas thermophila gen. nov., sp. nov., a
1020 novel thermophilic, hydrogen-oxidizing chemolithoautotroph within the epsilon-
1021 Proteobacteria, isolated from a black smoker in a Central Indian Ridge hydrothermal field. *Int*
1022 *J Syst Evol Microbiol* 54:25–32.
1023 52. Campbell BJ, Engel AS, Porter ML, Takai K. 2006. The versatile epsilon-proteobacteria: key
1024 players in sulphidic habitats. *Nat Rev Microbiol* 4:458–468.
1025 53. Sievert SM, Hügler M, Taylor CD, Wirsen CO. 2008. Sulfur oxidation at deep-sea
1026 hydrothermal vents, p. 238–258. *In* Microbial Sulfur Metabolism. Springer Berlin Heidelberg,
1027 Berlin, Heidelberg.
1028 54. Wommack KE, Williamson SJ, Sundbergh A, Helton RR, Glazer BT, Portune K, Craig Cary
1029 S. 2004. An instrument for collecting discrete large-volume water samples suitable for
1030 ecological studies of microorganisms. *Deep Sea Res Part I* 51:1781–1792.

1031 55. Bolger AM, Lohse M, Usadel B. 2014. Trimmomatic: a flexible trimmer for Illumina sequence
1032 data. *Bioinformatics* 30:2114–2120.
1033 56. Lo C-C, Chain PSG. 2014. Rapid evaluation and quality control of next generation
1034 sequencing data with FaQCs. BMC Bioinformatics 15:366.
1035 57. Ewels P, Magnusson M, Lundin S, Käller M. 2016. MultiQC: summarize analysis results for
1036 multiple tools and samples in a single report. *Bioinformatics* 32:3047–3048.
1037 58. Peng Y, Leung HCM, Yiu SM, Chin FYL. 2012. IDBA-UD: a de novo assembler for single-
1038 cell and metagenomic sequencing data with highly uneven depth. *Bioinformatic*s 28:1420–
1039 1428.
1040 59. Mikheenko A, Saveliev V, Gurevich A. 2016. MetaQUAST: evaluation of metagenome
1041 assemblies. *Bioinformatics* 32:1088–1090.
1042 60. Bray NL, Pimentel H, Melsted P, Pachter L. 2016. Near-optimal probabilistic RNA-seq
1043 quantification. *Nat Biotechno*l 34:888.
1044 61. R Core Team. 2021. *R: A language and environment for statistical computing*. R Foundation
1045 for Statistical Computing, Vienna, Austria.
1046 62. Wickham H, François R, Henry L, Müller K. 2023. *dplyr: A grammar of data manipulation*.
1047 R package version 1.1.3. https://CRAN.R-project.org/package=dplyr
1048 63. Li D, Liu C-M, Luo R, Sadakane K, Lam T-W. 2015. MEGAHIT: an ultra-fast single-node
1049 solution for large and complex metagenomics assembly via succinct de Bruijn graph.
1050 *Bioinformatics* 31:1674–1676.
1051 64. Kang DD, Li F, Kirton E, Thomas A, Egan R, An H, Wang Z. 2019. MetaBAT 2: an adaptive
1052 binning algorithm for robust and efficient genome reconstruction from metagenome
1053 assemblies. *PeerJ* 7:e7359.

1054 65. Li H. 2013. Aligning sequence reads, clone sequences and assembly contigs with BWA-MEM.
1055 *arXiv*.
1056 66. Li H, Handsaker B, Wysoker A, Fennell T, Ruan J, Homer N, Marth G, Abecasis G, Durbin
1057 R, 1000 Genome Project Data Processing Subgroup. 2009. The Sequence Alignment/Map
1058 format and SAMtools. *Bioinformatics* 25:2078–2079.
1059 67. Sieber CMK, Probst AJ, Sharrar A, Thomas BC, Hess M, Tringe SG, Banfield JF. 2018.
1060 Recovery of genomes from metagenomes via a dereplication, aggregation and scoring strategy.
1061 *Nat Microbio*l 3:836–843.
1062 68. Chaumeil P-A, Mussig AJ, Hugenholtz P, Parks DH. 2022. GTDB-Tk v2: memory friendly
1063 classification with the genome taxonomy database. *Bioinformatics* 38:5315–5316.
1064 69. Magoč T, Salzberg SL. 2011. FLASH: fast length adjustment of short reads to improve genome
1065 assemblies. *Bioinformatics* 27:2957–2963.
1066 70. Kopylova E, Noé L, Touzet H. 2012. SortMeRNA: fast and accurate filtering of ribosomal
1067 RNAs in metatranscriptomic data. *Bioinformatics* 28:3211–3217.
1068 71. Schloss PD, Westcott SL, Ryabin T, Hall JR, Hartmann M, Hollister EB, Lesniewski RA,
1069 Oakley BB, Parks DH, Robinson CJ, Sahl JW, Stres B, Thallinger GG, Van Horn DJ, Weber
1070 CF. 2009. Introducing mothur: open-source, platform-independent, community-supported
1071 software for describing and comparing microbial communities. *Appl Environ Microbiol*
1072 75:7537–7541.
1073 72. Wickham H. 2016. *ggplot2: Elegant Graphics for Data Analysis*. Springer-Verlag, New York,
1074 NY.
1075 73. Wickham H, Averick M, Bryan J, Chang W, D'Agostino McGowan L, François R, Grolemund
1076 G, Hayes A, Henry L, Hester J, Kuhn M, Lin Pedersen T, Miller E, Bache SM, Müller K, Ooms

1077 J, Robinson D, Seidel DP, Spinu V, Takahashi K, Vaughan D, Wilke C, Woo K, Yutani H.
1078 2019. *Welcome to the tidyverse*. J Open Source Softw 4:1686.
1079 https://doi.org/10.21105/joss.01686
1080 74. Li B, Dewey CN. 2011. RSEM: accurate transcript quantification from RNA-Seq data with or
1081 without a reference genome. BMC Bioinformatics 12:323. https://doi.org/10.1186/1471-2105-
1082 12-323
1083 75. Takahashi S, Tomita J, Nishioka K, Hisada T, Nishijima M. 2014. Development of a
1084 prokaryotic universal primer for simultaneous analysis of Bacteria and Archaea using next-
1085 generation sequencing. *PLoS One* 9:e105592.
1086 76. Crump BC, Kling GW, Bahr M, Hobbie JE. 2003. Bacterioplankton community shifts in an
1087 arctic lake correlate with seasonal changes in organic matter source. *Appl Environ Microbiol*
1088 69:2253–2268.
1089 77. Zhou J, Bruns MA, Tiedje JM. 1996. DNA recovery from soils of diverse composition. *Appl*
1090 *Environ Microbiol 62*:316–322.